

QATAR EXOPLANET SURVEY: QATAR-7B – A VERY HOT JUPITER ORBITING A METAL RICH F-STAR

KHALID ALSUBAI,¹ ZLATAN I. TSVETANOV,¹ DAVID W. LATHAM,² ALLYSON BIERYLA,² STYLIANOS PYRZAS,¹ DIMITRIS MISLIS,¹
GILBERT A. ESQUERDO,² ALI ESAMDIN,³ JINZHONG LIU,³ LU MA,³ MARC BRETTON,⁴ ENRIC PALLÉ,^{5,6} FELIPE MURGAS,^{5,6}
NICOLAS P. E. VILCHEZ,¹ TIMOTHY D. MORTON,⁷ HANNU PARVIAINIEN,^{5,6} PILAR MONTAÑES-RODRIGUEZ,^{5,6} NORIO NARITA,^{8,9}
AKIHIKO FUKUI,^{8,9} NOBUHIKO KUSAKABE,⁹ AND MOTOHIDE TAMURA^{8,9}

¹*Hamad bin Khalifa University (HBKU), Qatar Foundation, PO Box 5825, Doha, Qatar*

²*Harvard-Smithsonian Center for Astrophysics, 60 Garden Street, Cambridge, MA 02138, USA*

³*Xinjiang Astronomical Observatory (XAO), Chinese Academy of Sciences, 150 Science 1-Street, Urumqi, Xinjiang 830011, China*

⁴*Observatoire des Baronnies Provençales (OBP), Le Mas des Grés, Route de Nyons, 05150 Moydans, France*

⁵*Instituto de Astrofísica da Canarias (IAC), 38205 La Laguna, Tenerife, Spain*

⁶*Departamento de Astrofísica, Universidad de La Laguna (ULL), 38206 La Laguna, Tenerife, Spain*

⁷*Astronomy Department, University of Florida, Gainesville, FL 32611, USA*

⁸*Department of Astronomy, Graduate School of Science, The University of Tokyo, 7-3-1 Hongo, Bunkyo-ku, Tokyo 113-0033, Japan*

⁹*Astrobiology Center, National Institutes of Natural Sciences, 2-21-1 Osawa, Mitaka, Tokyo 181-8588, Japan*

(Received 26 April 2018; Revised 8 July 2018; Accepted 10 December 2018)

Submitted to AJ

ABSTRACT

We present the discovery of Qatar-7b — a very hot and inflated giant gas planet orbiting close its parent star. The host star is a relatively massive main sequence F-star with mass and radius $M_{\star} = 1.41 \pm 0.03 M_{\odot}$ and $R_{\star} = 1.56 \pm 0.02 R_{\odot}$, respectively, at a distance $d = 726 \pm 26$ pc, and an estimated age ~ 1 Gyr. With its orbital period of $P = 2.032$ days the planet is located less than 5 stellar radii from its host star and is heated to a high temperature $T_{\text{eq}} \approx 2100$ K. From a global solution to the available photometric and radial velocity observations, we calculate the mass and radius of the planet to be $M_{\text{p}} = 1.88 \pm 0.25 M_{\text{J}}$ and $R_{\text{p}} = 1.70 \pm 0.03 R_{\text{J}}$, respectively. The planet radius and equilibrium temperature put Qatar-7b in the top 6% of the hottest and largest known exoplanets. With its large radius and high temperature Qatar-7b is a valuable addition to the short list of targets that offer the best opportunity for studying their atmospheres through transmission spectroscopy.

Keywords: techniques: photometric - planets and satellites: detection - planets and satellites: fundamental parameters - planetary systems.

1. INTRODUCTION

While the detection of a habitable, Earth-like planet is undoubtedly seen as the "Holy Grail" of exoplanet research, hot Jupiters have enjoyed significant attention for many years and are still actively pursued. It is these gas giant planets, containing the bulk of the planetary system mass, that drive the shaping and final configuration of the planetary system. With growing numbers, statistical studies of populations became feasible, and intense efforts have been devoted into investigating possible correlations between the gas giants and the properties of their host stars, such as e.g., the now well-established positive correlation with the host's metallicity showing that hot Jupiters orbit stars with preferentially super-solar metallicities (e.g., [Ida & Lin 2004](#), [Fisher & Valenti 2005](#), [Mordasini et al. 2012](#); see also [Maldonado et al. 2013](#), [Reffert et al. 2015](#), [Santos et al. 2017](#), [Buchhave et al. 2018](#)).

Another important consideration in the framework of gas giant occurrence, is the role of the mass of the central star. Models of planet formation (see e.g., [Ida & Lin 2005](#); [Kennedy & Kenyon 2008](#)) suggest a positive correlation, i.e., that the giant planet frequency increases with increasing stellar mass. While this prediction seems to be supported by observations in the solar-like, main-sequence (MS) FGK regime (e.g., [Cumming et al. 2008](#)), it remains largely unvalidated in the MS-AF regime (with $M_{\star} \sim 1.2 - 3.5 M_{\odot}$), mainly because of the technical difficulties in measuring Doppler radial velocity (RV) in MS-AF spectra, due to lack of spectral absorption lines and fast rotation.

To overcome this problem, GK-subgiants and giants have been used as proxys, based on the assumption that they are equally massive with- and descendants of MS-AF dwarfs (e.g. [Johnson et al. 2007, 2008, 2010a](#)), while having the advantages of being cooler (and therefore exhibiting more absorption lines) and less-rapidly rotating, allowing standard Doppler RV measurements. One of the main findings reported was an obvious paucity of gas giants at small separations (≤ 1 AU) around subgiant and giant stars, compared to solar-like dwarfs (e.g. [Bowler et al. 2010](#); [Johnson et al. 2010b](#); [Reffert et al. 2015](#)). Plausible mechanisms involving disk dispersal/depletion timescales versus Type-II migration ([Papaloizou et al. 2007](#)) timescale have been investigated (e.g. [Burkert & Ida 2007](#), [Currie 2009](#); see also [Ribas et al. 2015](#)). We note however that some authors have challenged the validity of the assumptions regarding the mass of GK-subgiants and giants ([Lloyd 2011](#)), and proposed an alternative mechanism (albeit not necessarily mutually exclusive) involving orbital decay and tidal destruction (e.g. [Schlaufman & Winn 2013](#); [Villaver et al. 2014](#)), sparking a debate on evolutionary models ([Johnson et al. 2013](#); [Lloyd 2013](#)).

In the above context, main-sequence AF stars can become targets of choice and provide crucial input into the impact of the host star's mass on the frequency and period distribution of gas giant planets, in the intermediate M_{\star} regime. Driven by a few transit-detections (OGLE2-TR-L9: [Snellen et al. 2009](#); WASP-33b: [Collier Cameron et al. 2010](#); CoRoT-11b: [Gandolfi et al. 2010](#); KOI-13: [Rowe et al. 2011](#), [Mislis & Hodgkin 2012](#); KELT-9b: [Gaudi et al. 2017](#); KELT-20b: [Lund et al. 2017](#); MASCARA-2b: [Talens et al. 2018](#)) and a dedicated RV survey ([Borngiet et al. 2017](#), and the rest of the papers in the series), close-in gas giants (hot Jupiters) around $M_{\star} \geq 1.5 M_{\odot}$ stars have started gaining in numbers, although their area of the parameter space remains underpopulated, particularly in the short period ($P \leq 5$ d) regime.

In this article we present the discovery of Qatar-7b — a (very) hot Jupiter transiting a fast rotating F-star — found by the Qatar Exoplanet Survey (QES) The structure of the paper is as follows: in Section 2 we describe the observations – both the discovery photometry and the follow-up spectroscopy and photometry. In Section 3 we discuss the data analysis and the global system solution using simultaneous fits of the RV and transit light curves. The results are summarized in Section 4.

2. OBSERVATIONS

2.1. Discovery photometry

The survey data were collected with QES, hosted by the New Mexico Skies Observatory¹, Mayhill, NM, USA. A detailed description of QES can be found in our previous publications, e.g., [Alsubai et al. \(2013\)](#), [Alsubai et al. \(2017\)](#). In brief, QES uses two overlapping wide field 135 mm (f/2.0) and 200 mm (f/2.0) telephoto lenses, together with four 400 mm (f/2.8) telephoto lenses, mosaiced to image an $11^{\circ} \times 11^{\circ}$ field on the sky. Each lens is equipped with a FLI ProLine PL16801 camera utilizing a KAF-16801E 4k×4k detector.

The discovery light curve of Qatar-7b contains $\sim 11\,000$ data points obtained with one of the 400 mm lenses from October 2012 to December 2014. The data were reduced with the QES pipeline, which performs bias-correction, dark-current subtraction and flat-fielding in the standard fashion, while photometric measurements are extracted using the image subtraction algorithm by [Bramich \(2008\)](#); a more detailed description of the pipeline is given in [Alsubai et al. \(2013\)](#).

¹ <http://www.nmskies.com>

Table 1. Log of follow-up transit observations for Qatar-7b. See text for details on telescopes/instruments.

Obs ID	Date	Telescope	Filter	Cadence, s
1	2017-09-24	FLWO	i	35
2	2017-10-16	NOWT	i	30
3	2017-10-24	OBP	I	125
4	2017-11-06	FLWO	i	84
5	2017-11-06	FLWO	V	84
6	2017-12-24	OBP	I	125
7	2017-12-26	TCS	g	30
8	2017-12-26	TCS	r	30
9	2017-12-26	TCS	i	30
10	2017-12-26	TCS	z	30
11	2018-01-08	QFT	g	204

The extracted light curves are detrended using a combination of the Trend Filtering Algorithm (TFA, Kovács et al. 2005) and the Doha algorithm (Mislis et al. 2017). Qatar-7b was identified as a strong candidate during a search for transit-like events using the Box Least Squares algorithm (BLS, Kovács et al. 2002), following a procedure similar to that described in Collier Cameron et al. (2006). Note that, although the initial candidate selection is an automatic procedure, the final vetting is done by eye.

2.2. Follow-up photometry

Follow-up photometric observations of several transits of Qatar-7b were collected at five different observatories with the following combination of telescopes and instruments: (a) FLWO: we used the 1.2 m telescope at the Fred L. Whipple Observatory (Mount Hopkins, Arizona), together with KeplerCam, a $4K \times 4K$ CCD, with an on-sky FOV of $23' \times 23'$; (b) QFT: we used the 0.5 m Qatar Follow-Up Telescope (New Mexico Skies Observatory, Mayhill, New Mexico), equipped with a $1k \times 1k$ Andor iKon-M 934 CCD, yielding a FOV of $13' \times 13'$; (c) OBP: we used the 0.82 m telescope of the Observatoire des Baronnies Provençales² (Provence-Alpes-Côte d'Azur, France), equipped with an FLI ProLine PL230 CCD, with a $2k \times 2k$ E2V detector, resulting in a $23' \times 23'$ FOV; and (d) XAO: we used the Nanshan One-meter Wide-field Telescope (NOWT) of the Xinjiang Astronomical Observatory (XAO) equipped with a $4k \times 4k$ CCD with full on-sky FOV of $1.28^\circ \times 1.28^\circ$. To shorten the readout time and increase the duty cycle only a 1200×1200 pixels subframe was used resulting in a $22.5' \times 22.5'$ area on the sky. (e) TCS: we used the 1.52 m Telescopio Carlos Sanchez (TCS) at the Teide Observatory (Tenerife, Canary Islands), and MuSCAT2 instrument, which takes images in 4 filters simultaneously. Each channel is equipped with a $1K \times 1K$ CCD, resulting in a $7.4' \times 7.4'$ on-sky FOV. For a detailed description of MuSCAT2 and its dedicated photometric pipeline see Narita et al. (2018).

A summary of our follow-up photometric observations is given in Table 1. The resulting light curves, along with the best model fit and the corresponding residuals, are plotted in Figure 1.

2.3. Follow-up spectroscopy

Follow-up spectroscopic observations for Qatar-7b were obtained in the same manner as for all other QES candidates. We used the Tillinghast Reflector Echelle Spectrograph (TRES) on the 1.5 m Tillinghast Reflector at FLWO. The light from the object was fed to the spectrograph through the medium fiber, resulting in a resolving power of $R \sim 44,000$ and a velocity resolution element of 6.8 km s^{-1} FWHM. Two exposures of a Th-Ar hollow-cathode lamp illuminating the science fiber were taken immediately before and after each science spectrum to establish precise wavelength calibration.

For Qatar-7 we obtained 14 spectra between August 28, 2017 – February 8, 2018 with exposure times in the range 30–60 min resulting in an average signal-to-noise ratio per resolution element (SNRe) of ~ 25 at the peak of the continuum close to the Mg b triplet near 519 nm. We selected the best spectrum as our reference one, and measured relative radial velocities (RV) using the cross-correlation technique; under this framework, a specific set of echelle orders is chosen, meeting the following two criteria (i) good SNRe and (ii) minimal telluric lines contamination. All the observed spectra subsequently undergo order by order cross-

² <http://www.obs-bp.fr>

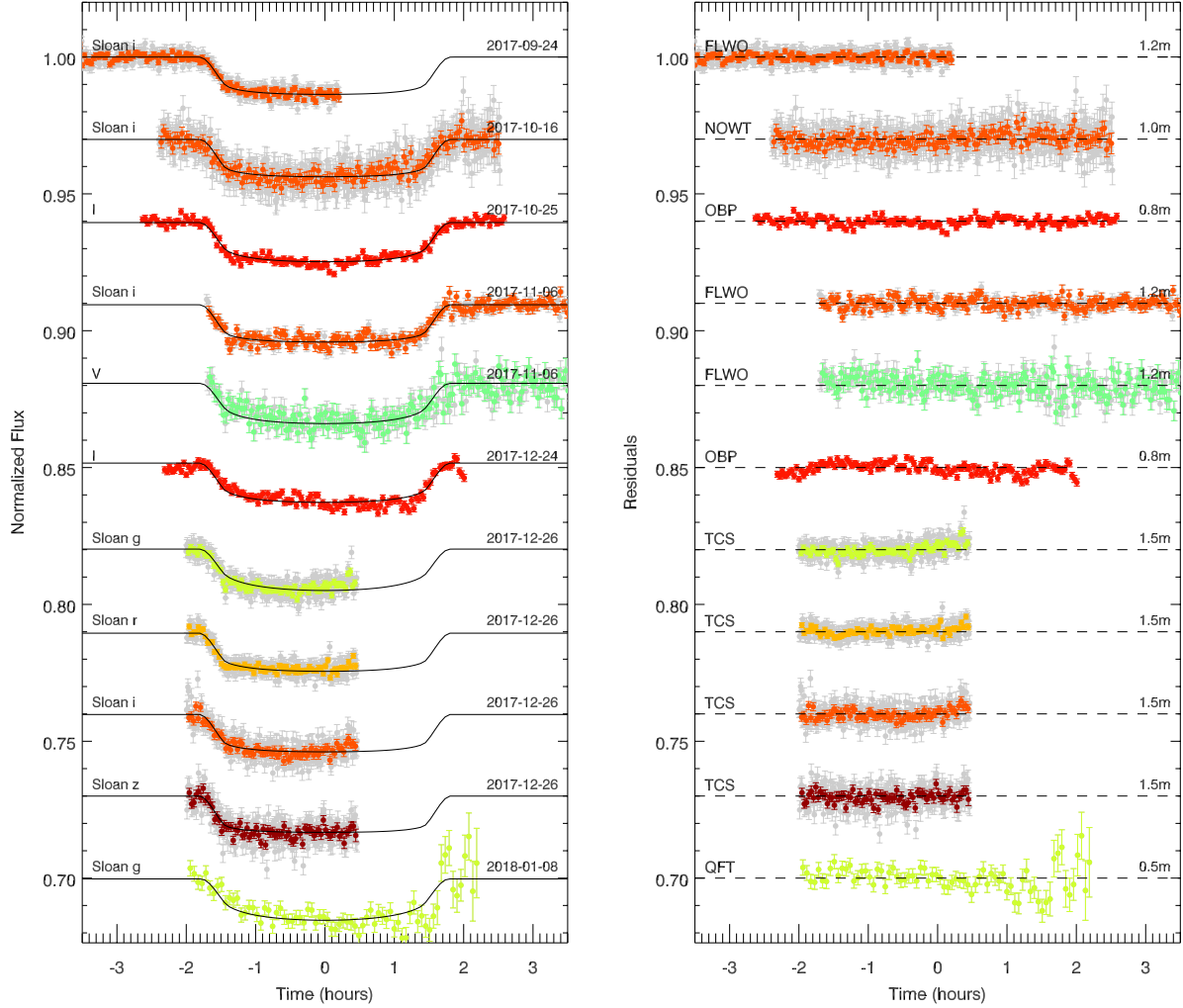


Figure 1. The eleven follow-up transit light curves of Qatar-7b. In the *left* panel, the light curves are ordered from top to bottom as they appear in Table 1 and have been shifted vertically for clarity. The solid, black lines represent the best model fit (see Section 3.4). The residuals from the fits are shown in the *right* panel. The individual data points are color coded according to the filter used and for observations taken at FLWO, XAO and Teide observatories we show both the original data points (light gray) as well as the data binned to a uniform cadence of 2 min, while for observation taken at OBP and QFT we only show the original data points as their cadence is ≥ 2 min. The filter, date of observation, observatory and telescope size are also given in the two panels.

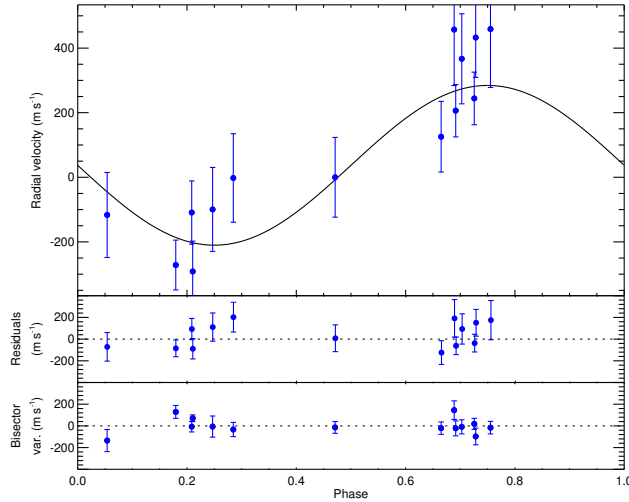
correlation against the reference spectrum. By default, the RV value of the reference spectrum is zero, while the error assigned to this value is simply the median of all other errors of our RV measurements. In order to exclude other astrophysical phenomena, that could potentially mimic the orbital-motion induced periodic signal evident in our RV measurements, we also calculated the line profile bisector spans (BS). The full process of measuring the RVs and BSs is described in detail in Buchhave et al. (2010). We collect the RV and BS values in Table 2 and plot them in Figure 2.

3. ANALYSIS AND RESULTS

3.1. The host star

Table 2. Relative RVs and BS variations for Qatar-7.

BJD_{TDB}	RV (m s^{-1})	BS (m s^{-1})
2457993.94705	366.9 ± 139.5	-9.0 ± 65.0
2457994.91573	-271.6 ± 77.2	129.0 ± 59.3
2458034.63495	244.2 ± 81.5	18.7 ± 50.8
2458035.61646	-109.1 ± 97.8	-7.1 ± 48.7
2458037.80307	-2.2 ± 137.0	-33.5 ± 65.6
2458039.68421	-291.6 ± 93.9	70.2 ± 30.8
2458040.60790	125.6 ± 109.4	-21.1 ± 57.3
2458042.69416	206.3 ± 81.1	-22.6 ± 68.9
2458095.60236	432.7 ± 123.5	-97.6 ± 77.1
2458107.71464	457.4 ± 173.3	144.9 ± 85.8
2458116.58480	-116.6 ± 131.6	-135.2 ± 102.0
2458127.59278	-0.0 ± 123.5	-14.3 ± 54.1
2458156.61948	458.9 ± 180.8	-16.2 ± 57.8
2458157.61827	-99.5 ± 130.1	-6.4 ± 97.6

**Figure 2.** Orbital solution for Qatar-7b, showing the velocity curve and observed velocities and the bisector values.

The host star of Qatar-7b (2MASS J23540364+3701185, henceforth Qatar-7) is a relatively faint, $V = 13.03$ mag, mid-to-late F-type star³. In what follows, we present our analysis of the host star, while Table 3 presents a comprehensive summary.

3.1.1. Spectroscopic parameters

To determine the host star atmospheric characteristics – effective temperature (T_{eff}), surface gravity ($\log g$), and metallicity ($[\text{Fe}/\text{H}]$), as well as the projected rotational velocity (v_{rot}) – we analyzed the available spectroscopic data used for the RV measurements (see Section 2.3) through the Stellar Parameter Classification tool (SPC, Buchhave et al. 2012)). Because individual TRES spectra have relatively low S/N ratio, all 14 spectra were wavelength shifted and co-added to form a high signal-to-noise spectrum representative of the host star.

³ An estimate from a multi-color fit to the V , J , H and K magnitudes, using a standard Random-Forest classification algorithm

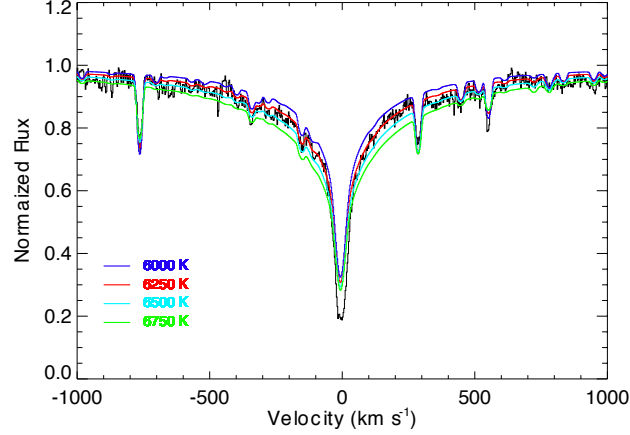


Figure 3. $H\alpha$ profile from the combined spectrum of Qatar-7 compared with four synthetic spectra with $[\text{Fe}/\text{H}]=0.25$, $\log g=4.2$ and $T_{\text{eff}}=6000$, 6250, 6500, and 6750 K, respectively.

The SPC determines the stellar parameters from a multi-dimensional surface fit to the cross correlation of the observed spectrum with a library of Kurucz synthetic spectra (Castelli & Kurucz 2004). The SPC determined values are: $T_{\text{eff}} = 6311 \pm 50$ K, $\log g = 4.26 \pm 0.10$, $[\text{Fe}/\text{H}] = 0.29 \pm 0.08$, and line broadening $v_{\text{l.b.}} = 14.7 \pm 0.5$ km s $^{-1}$.

In solar type main sequence stars the wings of the $H\alpha$ line profile have strong sensitivity to temperature variations and at the same time relatively weak sensitivity to changes in the surface gravity and metallicity, which makes this feature a good temperature indicator (e.g., Fuhrmann et al. 1993; Barklem et al. 2002). As a consistency check on T_{eff} we compared the observed $H\alpha$ profile outside the core in the co-added spectrum to synthetic spectra generated with the Spectroscopy Made Easy package (SME, Valenti & Piskunov 1996) using the Kurucz ATLAS9 grid of models. Template spectra were generated with $\log g = 4.2$, $[\text{Fe}/\text{H}] = 0.25$ and $T_{\text{eff}} = 6000$, 6250, 6500, and 6750 K. In Figure 3, in velocity space, we show the observed $H\alpha$ profile and the four synthetic spectra. It is clear the $H\alpha$ line profile is best reproduced by synthetic spectra with T_{eff} in the range 6250–6500 K. We note here, that the shape of the observed $H\alpha$ profile is sensitive to the continuum normalization, which is difficult to pinpoint for such a broad line in an echelle spectrum. For that reason, we consider this comparison only as a rough check on T_{eff} , yet, it agrees with our previous estimates.

3.1.2. SED fit

Qatar-7 is detected by most of the large-scale surveys and, as such, photometric measurements are available across the spectrum, from the NUV (GALEX) to the mid-IR (WISE). These measurements are gathered in Table 3. We note that for the Sloan u, g, r, i, z bands, the *actual* SDSS photometry⁴ is classified as “unreliable”, accompanied by a variety of cautionary flags primarily related to saturated and interpolated pixels. To ameliorate the problem, we turned to the APASS catalogue (Henden et al. 2015) and the work of Pickles & Depagne (2010) (PD10) and adopt the g, r, i values from APASS and the u, z values from PD10.

We used the broadband measurements combined with the distance measured by *Gaia* to fit a SED using the NextGen library of theoretical models and solve for the extinction and stellar radius R_{\star} . We note that the shape of the SED is determined by the T_{eff} and extinction, while the value of R_{\star} is dependent on the distance. In fitting the SED we imposed a Gaussian prior of 0.05 on the extinction mean value of $A_V \approx 0.35$ mag as suggested by the Galactic dust reddening maps (Schlafly & Finkbeiner 2011). Figure 4 shows that the SED of a $T_{\text{eff}} \sim 6400$ K main sequence star fits very well the broadband photometry for a distance $d = 720$ pc and extinction $A_V = 0.36$ mag (uncertainties are given in Table 3).

3.1.3. Age

To obtain an estimate of the age of Qatar-7, we used three different age indicators—gyrochronology, isochrone fitting, and lithium abundance. First, the star is a relatively fast rotator, which is indicative of a young age. For the gyrochronology method we applied the rotational period–color–age relations, as calibrated by Brown (2014), assuming the stellar rotation axis is perpendicular to the orbital plane of the planet. The stellar projected equatorial rotational velocity, $v \sin i$, was estimated from the line broadening, $v_{\text{l.b.}}$, measured by SPC and accounting for the macroturbulence velocity, v_{mac} , contribution. We estimated $v_{\text{mac}} = 5$

⁴ <http://skyserver.sdss.org/dr14>

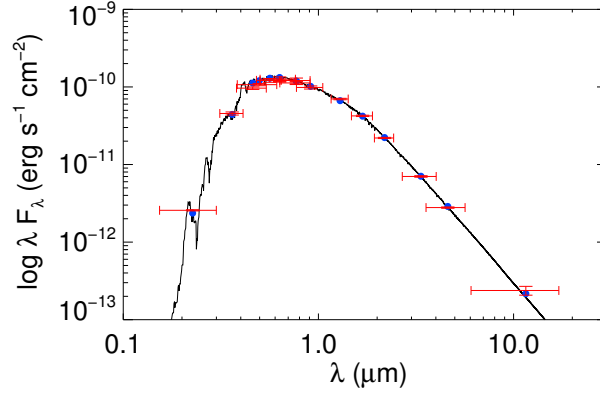


Figure 4. Spectral Energy Distribution (SED) fit for Qatar-7b host star. The 1σ uncertainties of the photometric measurements (Table 3) are plotted as vertical bars, and the effective width of the passbands is shown by horizontal bars. The solid curve is the best fit model SED where stellar parameters R_* , T_{eff} , $\log g$, and $[\text{Fe}/\text{H}]$ were kept fixed at the values derived from the global fit (Table 5).

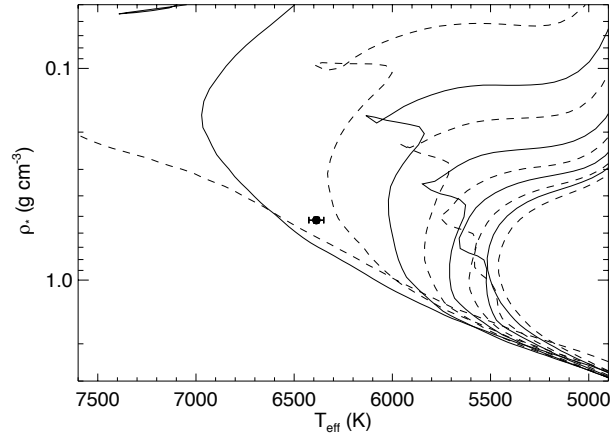


Figure 5. Model isochrones from the YY series (Yi et al. 2001) for the measured metallicity of Qatar-7b. Isochrones for ages 0.6 Gyr and 1.0–10.0 Gyr in 1 Gyr intervals are plotted in alternating dashed and solid lines. Ages are increasing left to right.

km s^{-1} using the calibrations of Meléndez et al. (2012) (average of their Eqs. (E.1) and (E.2) valid for the T_{eff} of our star) and assuming $v_{\text{mac}}^{\circ} = 3.6 \text{ km s}^{-1}$. As a result we adopted $v_{\text{rot}} \equiv v \sin i = (v_{\text{lb}}^2 - v_{\text{mac}}^2)^{1/2} = 13.8 \text{ km s}^{-1}$ for the rotational velocity and we used the reddening corrected values for the $B-V$ and $J-K$ colors. The gyrochronology estimated age is $\tau_{\text{gyr}} = 0.5 \pm 0.1 \text{ Gyr}$, where the uncertainty reflects only the errors in color measurements and determining the stellar rotation period.

An alternative estimate of the host star age can be obtained from comparing the observationally determined parameters T_{eff} and ρ_* with theoretical evolution models. Stellar effective temperature, T_{eff} , is determined from the spectroscopic analysis (Section 3.1.1) while stellar density, ρ_* , is derived from the transit light curves analysis. We note that the fit to the transit light curves is obtained by varying three parameters — the relative planet radius, R_p/R_* , the impact parameter, $b = a \cos i/R_*$, and the relative semi-major axis, a/R_* (see e.g., Mandel & Agol 2002, Pont et al. 2007). Using the Kepler’s third law and assuming $M_* \gg M_p$ and a circular orbit the density of the star is directly determined by a/R_* and the orbital period (e.g., Seager & Mallén-Ornelas 2003).

In Figure 5 we compare the stellar density ρ_* and T_{eff} with model isochrones from the Yi et al. (2001) database. The isochrones plotted are calculated for the metallicity suggested by the spectroscopic analysis, $[m/\text{H}] = 0.25 \pm 0.10$, and cover a wide range in age (0.6–12 Gyr). The best match to the observationally measured parameters ρ_* , T_{eff} is achieved for stellar age $\tau = 1.0 \pm 0.5 \text{ Gyr}$, where the uncertainty is driven by the observational errors.

In the course of the stellar evolution Li is destroyed at temperatures $\sim 2.5 \times 10^6 \text{ K}$ when it is transported to the innermost layers of the star through convective motions. Although the level of Li burning is controlled by several factors, e.g., convective zone

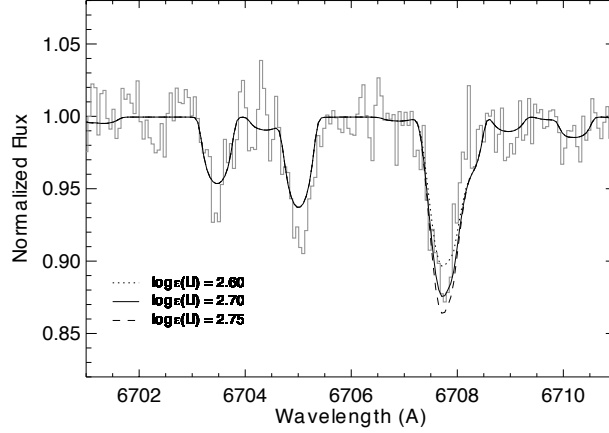


Figure 6. A portion of the co-added observed spectrum of Qatar-7b host star containing the Li I 6707.8 Å line plotted in gray. Overplotted are three synthetic spectra differing only by the Li abundance as depicted by lines of different style. The best fit to the Li I 6707.8 Å line requires $\log \epsilon(\text{Li}) = 2.70$.

thickness, stellar mass, and metallicity, the degree of Li depletion in stars depends primarily on the stellar age in the sense that older stars have lower Li abundance (e.g., Meléndez et al. 2014, Tucci Maia et al. 2015).

The resonance line Li I $\lambda 6707.8$ is by far the strongest Li feature in the optical and is the source of most of the Li abundance estimates. We note, that because of the low ionization potential (5.39 eV), Li I lines can only be seen in stars with $T_{\text{eff}} < 8500$ K. The host star of Qatar-7b displays a strong Li I $\lambda 6707.8$ absorption line indicative of a young age. We have carried out a spectral synthesis of a 10 Å region centered on the Li line using the SME package and the stellar atmospheric parameters obtained in Section 3.1.1. Figure 6 shows a comparison of the co-added spectrum of Qatar-7b with three synthetic spectra that differ only in Li abundance. The best fit is obtained for Li abundance of $\log \epsilon(\text{Li}) = 2.70$. By comparison with the Li abundance curves as a function of age for different T_{eff} for open clusters (Sestito & Randlich 2005) we estimate an age ≤ 1 Gyr for Qatar-7b host star.

To summarize, all three age estimates give values in the range 0.5-1.5 Gyr. A more precise age determination may be possible via asteroseismology but would require a photometric data set of much better precision. In Table 3 we quote the age of Qatar-7 as 1 Gyr, which is representative of the range of estimates, and put the uncertainty conservatively at 0.5 Gyr.

3.2. Orbital period determination

We used our follow-up light curves to determine the ephemeris of the system. From the eleven available light curves (as listed in Table 1) we did not include the 1st and 7-10th, because they are partial and cannot provide an *independent* measurement of T_C ; the 5th, because it's simultaneous with the 4th, but has larger scatter; and the 11th, because of insufficient coverage of out-of-transit parts.

For the remaining four light curves, we first converted all time-stamps to the BJD_{TDB} timescale and proceeded to fit each one individually using EXOFASTv2 (Eastman 2017). The resulting transit central times T_C and their uncertainties are listed in Table 4. The best ephemeris was calculated by fitting a straight line through the measured T_C points. The resulting orbital ephemeris is

$$T_C = 2458043.32075(16) + 2.032070(17) E \quad (1)$$

where E is the number of cycles after the reference epoch, which we take to be the y-intercept of the linear fit, and the numbers in parentheses denote the uncertainty in the last two digits. In Equation (1), the reference epoch and the period are in days on the BJD_{TDB} scale, and their uncertainties correspond to 14 s, and 1.5 s, respectively.

3.3. Excluding a false positive

Observational data described in the previous sections – the shape and depth of the transit light curves plus the shape and amplitude of the RV curve – can be described by a case of a planet orbiting a single star. Yet, there are other astrophysical scenarios that could mimic such a behaviour and include an eclipsing binary – either a background or in a hierarchical tripple system – blended with the primary (and brighter) star. Here we present arguments to exclude such scenarios and to prove that the observed behaviour is not a false positive.

Table 3. Basic observational and spectroscopic parameters of Qatar-7b host star and photometry used for the SED fit.

Parameter	Description	Value	Source	Ref.
Names				
	3UC 255-282464, 4UC 636-128328			
	SDSS J235403.63+370118.5, 2MASS J23540364+3701185			
	GALEX J235403.7+370119, WISE J235403.63+370118.6			
Astrometry				
α_{2000}	RA (J2000)	23 ^h 54 ^m 03.63 ^s	GAIA	1
δ_{2000}	DEC (J2000)	+37 ^o 01'18.57''	GAIA	1
π	parallax, mas	1.3884 ± 0.0501	GAIA	1
Photometry				
NUV	GALEX NUV, mag	18.18 ± 0.02	GALEX	2
<i>B</i>	Johnson <i>B</i> , mag	13.69 ± 0.04	APASS	4
<i>V</i>	Johnson <i>V</i> , mag	13.03 ± 0.06	APASS	4
<i>u</i>	Sloan <i>u</i> , mag	14.62 ± 0.05	PD10	3
<i>g</i>	Sloan <i>g</i> , mag	13.32 ± 0.04	APASS	4
<i>r</i>	Sloan <i>r</i> , mag	12.86 ± 0.08	APASS	4
<i>i</i>	Sloan <i>i</i> , mag	12.67 ± 0.08	APASS	4
<i>z</i>	Sloan <i>z</i> , mag	12.70 ± 0.01	PD10	3
<i>J</i>	2MASS <i>J</i> , mag	11.859 ± 0.023	2MASS	4
<i>H</i>	2MASS <i>H</i> , mag	11.599 ± 0.021	2MASS	4
<i>K</i>	2MASS <i>K</i> , mag	11.561 ± 0.020	2MASS	4
W1	WISE1, mag	11.481 ± 0.024	WISE	5
W2	WISE2, mag	11.504 ± 0.021	WISE	5
W3	WISE3, mag	11.252 ± 0.142	WISE	5
Spectroscopic parameters				
	Spectral type	F4V	this work	
T_{eff}	Effective temperature, K	6311±50	this work	
$\log g$	Gravity, cgs	4.26±0.10	this work	
[<i>m</i> /H]	Metallicity	0.29±0.08	this work	
γ_{abs}	Systemic velocity, km s ⁻¹	-4.7 ± 0.1	this work	
v_{rot}	Rotational velocity, km s ⁻¹	13.8±0.5	this work	
P_{rot}	Rotation period, days	5.9 ± 0.2	this work	
τ	Age, Gyr	1.0 ± 0.5	this work	
A_V	Extinction, mag	0.38 ± 0.05	S&F2011	8
<i>d</i>	Distance, pc	720 ± 26	GAIA	1

References—(1) GAIA DR2 <http://gea.esac.esa.int/archive/>,
(2) GALEX <http://galex.stsci.edu/>, (3) Pickles & Depagne (2010),
(4) APASS9 <http://www.aavso.org/apass/>,
(5) 2MASS <http://irsa.ipac.caltech.edu/Missions/2mass.html>,
(6) WISE <http://irsa.ipac.caltech.edu/Missions/wise.html>

Table 4. Central times of Qatar-7b transits and their uncertainties. The last column corresponds to the first column of Table 1.

Transit central time BJD _{TDB} - 2 450 000	Cycle No.	Obs ID
8043.32067 ± 0.00023	0	2
8051.44909 ± 0.00021	4	3
8063.64153 ± 0.00033	10	4
8112.41103 ± 0.00057	34	6

Our first argument comes from the behaviour of the spectral line bisectors (see Table 2). By now it is well understood (e.g., Queloz et al. 2001, Torres et al. 2005) that if measured radial velocities were a result of a blend with an eclipsing binary, the line bisectors would vary in phase with the photometric period and with an amplitude similar to that of the RV curve. As can be seen from bottom panel in Figure 2 in the case of Qatar-7 the line bisectors are essentially stationary throughout the photometric period. The weighted mean of the bisector distribution is $0 \pm 20 \text{ m s}^{-1}$, while the RV amplitude is $K = 239 \pm 32 \text{ m s}^{-1}$. This lends a strong argument that the observed RV pattern is a result of a gravitationally induced motion from a planet orbiting a single star.

A second argument supporting the planet scenario comes from the fact that transit light curves in all filters have equal depth after accounting for the limb darkening. In fact, our transit photometry is good enough to detect small differences in the depth due to the wavelength dependence of the limb darkening and the results are in full agreement with a central transit (depth decreases with wavelength) as expected given the estimated impact parameter b (Table 5). Equal transit depths at different wavelengths, however, do not preclude a scenario of a stellar companion of similar colors. For this reason, we consider this argument only as supportive of the planetary scenario, but note that it is in full agreement with the conclusion of this section.

Finally, we compute the False Positive Probability (FPP) for all scenarios involving an eclipsing binary using the *vespa* package (Morton 2012, Morton 2015). Originally, *vespa* was developed as a tool for statistical validation of planet candidates identified by the *Kepler* mission (e.g., Morton et al. 2016) and its successor *K2* (e.g., Crossfield et al. 2016, Mayo et al. 2018). *Vespa* calculates FPP via model selection among a number of physical scenarios that could potentially explain the transit signal: an unblended eclipsing binary (EB), a hierarchical-triple eclipsing binary (HEB), a background/foreground (chance-aligned) eclipsing binary (BEB), the double-period cases of all these eclipsing-binary scenarios, and finally the transiting planet scenario. The likelihoods and priors for each scenario are based on the shape of the transit signal, the star’s location in the Galaxy, and single-, binary-, and triple-star model fits to the observed photometric and spectroscopic properties of the star, as well as the Gaia parallax. Additional constraints come from direct imaging from the MuSCAT2 photometry (see Section 2.2), which puts limits on the presence of potentially blending stars, and from a limit on the secondary transit (non-)detection estimated from our discovery curve — phase folded and binned to the transit duration. We note also that all previous published uses of *vespa* have been on Kepler data, for which the photometric integration time per cadence is approximately 30 minutes — for this work, where our photometry has 2-minute cadence, we update *vespa* to be able to use a custom integration time, which is important because longer integration times significantly smooth out the ingress/egress times, especially for short-period planets (Kipping 2010). This updated version of *vespa* computes Qatar-7b to have about a 5% probability of being caused by the EB scenario (a faint low-mass star eclipsing the primary), and negligible probability for any of the other false-positive scenarios. However, our radial velocity measurements completely exclude the presence of such a stellar-mass close companion; hence, we can remove the EB scenario from consideration by *vespa*, leaving completely negligible probability that the signal could be caused by a false positive. The only viable scenario is that of a planet orbiting a single star.

3.4. Planetary system parameters

We derived the physical parameters of the Qatar-7 planetary system by running a global fit of the available transit light curves (Figure 1) and RV measurements (Table 2) using EXOFASTv2 (Eastman 2017, Rodriguez et al. 2017). The set of parameters used to initialize the fit consisted of the orbital ephemeris (Section 3.2), the stellar parameters (T_{eff} , $\log g$, $[M/H]$) as determined through SPC, as well as the distance (via the GAIA parallax) and age (Section 3.1.1). In addition, we set the visual extinction to $A_V=0.38$, based on the Galactic dust reddening maps (Schlafly & Finkbeiner 2011). Gaussian priors were imposed on all these parameters, with the mean values and standard deviations quoted in Table 3. Limb darkening coefficients (LDCs) were left free to vary, but also had a Gaussian prior imposed on them, with the mean value interpolated from the Claret & Bloemen (2011) tables (for the given filter of each transit light curve used) and a standard deviation of 0.05. Finally, we kept the system eccentricity

Table 5. Median values and 68% confidence intervals. We assume $R_{\odot}=696342.0$ km, $M_{\odot}=1.98855\times 10^{30}$ kg, $R_J = 69911.0$ km, $M_J=1.8986\times 10^{27}$ kg and 1 AU=149597870.7 km.

Parameter	Units	Qatar-7b
Stellar Parameters:		
M_*	Mass (M_{\odot})	1.409 ± 0.026
R_*	Radius (R_{\odot})	1.564 ± 0.021
L_*	Luminosity (L_{\odot})	3.66 ± 0.13
ρ_*	Density (g/cm^3)	0.521 ± 0.016
$\log(g_*)$	Surface gravity (cgs)	4.196 ± 0.029
T_{eff}	Effective temperature (K)	6387 ± 38
[Fe/H]	Metallicity	0.276 ± 0.071
τ_{YY}	Age (Gyr)	1.69 ± 0.25
A_V	Extinction (mag)	0.338 ± 0.055
d	Distance (pc)	725 ± 10
Planetary Parameters:		
P	Period (days)	2.032046 ± 0.0000097
a	Semi-major axis (AU)	0.0352 ± 0.0002
M_P	Mass (M_J)	1.88 ± 0.25
R_P	Radius (R_J)	1.70 ± 0.03
ρ_P	Density (g/cm^3)	0.502 ± 0.071
$\log(g_P)$	Surface gravity	3.224 ± 0.066
T_{eq}	Equilibrium Temperature (K)	2053 ± 15
Θ	Safronov Number	0.056 ± 0.008
RV Parameters:		
K	RV semi-amplitude (m/s)	239 ± 32
γ_{rel}	Systemic velocity (m/s)	106 ± 35
e	Eccentricity (fixed)	0
Primary Transit Parameters:		
R_P/R_*	Radius of planet in stellar radii	0.110 ± 0.001
a/R_*	Semi-major axis in stellar radii	4.84 ± 0.05
i	Inclination (degrees)	89.0 ± 1.0
b	Impact Parameter	0.08 ± 0.08
T_{14}	Total duration (days)	0.1491 ± 0.0009

fixed to zero, as the orbit circularization timescale (using the [Jackson et al. \(2008\)](#) equations) is calculated to be $\tau_{\text{circ}} \leq 0.07$ Gyr, much lower than the estimated age of the host star.

The results of the global fit are summarized in Table 5. The Safronov number is not used in the current paper and is provided in Table 5 for completeness, as it may be useful for other studies.

4. DISCUSSION AND CONCLUSIONS

In this article, we present Qatar-7b, a newly identified very hot Jupiter orbiting close to a moderately fast rotating F-star. From a global fit to the available photometric and spectroscopic follow-up observations we measure the planet's mass $1.88 M_J$ and radius $1.70 R_J$, which puts Qatar-7b in the top 6% of the distribution of known exoplanets by size. With an orbital period $P = 2.032$ d,

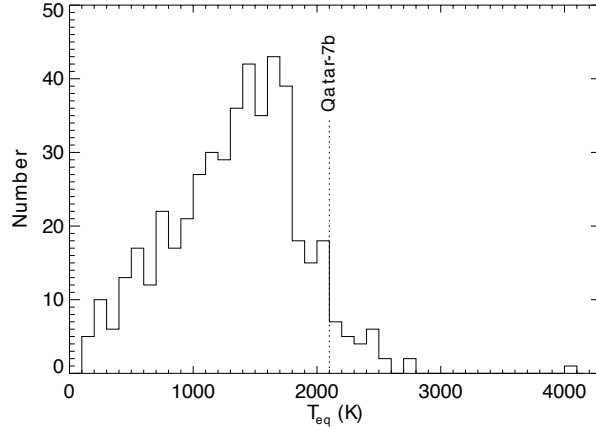


Figure 7. Histogram of the equilibrium temperature of exoplanets.

the planet is located only $4.84 R_{\star}$ from the host star and is heated to a very high equilibrium temperature $T_{\text{eq}} \approx 2100$ K putting it also within the top $\sim 6\%$ of the hottest known exoplanets.

Close-in transiting giant planets offer the best opportunities to look for dynamic interactions that may provide important information related to planetary system architecture and evolution. These include studies of the spin/orbit alignment through Rossiter-McLaughlin (RM) effect (Rossiter 1924, McLaughlin 1924) or Doppler Tomography (see Zhou et al. 2016a, Zhou et al. 2016b, Zhou et al. 2017) and the search for presence of additional bodies in the system that may be revealed through transit timing and/or transit duration variations (Kipping 2010). In addition, close-in transiting planets are often inflated due to the proximity and intense irradiation by the parent star, and are the best targets to study the atmospheric composition in extrasolar planets (see Murgas et al. 2017 and references therein).

By its characteristics, Qatar-7b is an excellent target for dynamical studies. The host is a fast rotating star, $v \sin i \approx 15 \text{ km s}^{-1}$ and combined with the relevant stellar and planetar parameters the predicted semi-amplitude of the RM effect is $\sim 200 \text{ m s}^{-1}$. With modern precision RV instruments the shape of the curve is expected to be securely measurable and allow for a good estimate of the stellar obliquity in the system. And last but not least, Qatar-7b is also an excellent target for atmospheric studies via transmission spectroscopy due to its significantly inflated planetary radius and very high equilibrium temperature. In Figures 7 and 8, using data for the well studied exoplanets from TEPcat⁵, we show that Qatar-7b falls within the top $\sim 6\%$ of the hottest exoplanets known so far and occupies a place close to the extreme end of the $R_{\text{P}}/T_{\text{eq}}$ relation.

In their study for HAT-P-65b and HAT-P-66b, Hartman et al. (2016) find that large, inflated hot Jupiters ($R_{\text{P}} > 1.5 R_{\text{J}}$) are preferentially found around older and/or slightly evolved stars. Defining the fractional age of the host star as $\tau = (t_{\text{cur}} - 200 \text{ Myr}) / (t_{\text{tot}} - 200 \text{ Myr})$, with t_{cur} and t_{tot} being the current and total lifetime of the star respectively, they find that the majority of stars hosting large hot Jupiters have $\tau > 0.5$, i.e., that they have spent more than half of their main-sequence lifetime. With a radius of $R_{\text{P}} = 1.70 R_{\text{J}}$, Qatar-7b comfortably falls in this category, but seems not to conform with the aforementioned trend, as the fractional age of the host star is calculated to be $\tau \approx 0.3$, for a total lifetime of $t_{\text{tot}} \approx 3.5 \text{ Gyr}$, as tabulated from the YY isochrones for a star of the same mass and metallicity.

ACKNOWLEDGEMENTS

This publication is supported by NPRP grant no. X-019-1-006 from the Qatar National Research Fund (a member of Qatar Foundation). The statements made herein are solely the responsibility of the authors. The Nanshan 1m telescope of XAO is supported by the CAS "Light of West China" program (XBBS-2014-25,2015-XBQN-A-02), and the Youth Innovation Promotion Association CAS (2014050). This article is partly based on observations made in the Observatorios de Canarias del IAC with the MUSCAT2 instrument on the Carlos Sanchez telescope operated on the island of Tenerife by the IAC in the Observatorio del Teide. This work is partly financed by the Spanish Ministry of Economics and Competitiveness through grants ESP2013-48391-C4-2-R. This work has made use of data from the European Space Agency (ESA) mission *Gaia* (<https://www.cosmos.esa.int/gaia>), processed by the *Gaia* Data Processing and Analysis Consortium (DPAC,

⁵ The Transiting Extrasolar Planet Catalog (TEPcat) is available at <http://www.astro.keele.uk/jkt/tepcat>

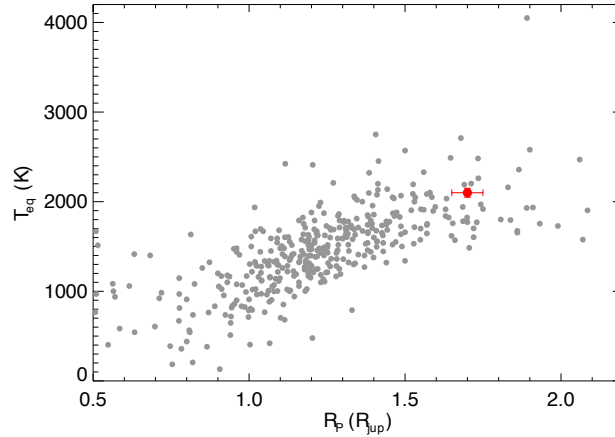


Figure 8. The planet radius–equilibrium temperature, R_p/T_{eq} , relation for exoplanets. The position of Qatar-7b is plotted with larger red symbol with error bars.

<https://www.cosmos.esa.int/web/gaia/dpac/consortium>). Funding for the DPAC has been provided by national institutions, in particular the institutions participating in the *Gaia* Multilateral Agreement. We also acknowledge support from JSPS KAKENHI Grant Number 16K13791.

REFERENCES

- Alsubai, K., Parley, N. R., Bramich, D. M., Horne, K., et al., 2013, *Acta Astron.*, 63, 465
- Alsubai, K., Mislis, D., Tsvetanov, Z. I., Latham, D. W., et al., 2017, *AJ*, 153, 200
- Barklem, P. S., Stempels, H. C., Allende Prieto, C., Kochukhov, O. P., et al., 2002, *A&A*, 385, 951
- Borgniet, S., Lagrange, A.-M., Meunier, N., & Galland, F., 2017, *A&A*, 599, 57B
- Bowler, B.P., Johnson, J. R., Marcy, G. W., Henry, G. W., et al., 2010, *ApJ*, 709, 396
- Bramich, D. M., 2008, *MNRAS*, 386, L77
- Brown, D. J. A., 2014, *MNRAS*, 442, 1844
- Buchhave, L. A., Bakos, G. Á., Hartman, J. D., Torres, G., et al., 2010, *ApJ*, 720, 1118
- Buchhave, L. A., Latham, D. W., Johansen, A., Bizzarro, M., et al., 2012, *Nature*, 486, 375
- Buchhave, L. A., Bitsch, B., Johansen, A., Latham, D., et al., 2018, *ApJ*, 856, 37
- Burkert, A., & Ida, S., 2007, *ApJ*, 660, 845
- Castelli, F. & Kurucz, R. L., 2004, astro-ph/0405087
- Claret, A. & Bloemen, S., 2011, *A&A*, 529, 75
- Collier Cameron, A., Pollacco, D., Street, R. A., Lister, T. A., et al., 2006, *MNRAS*, 373, 799
- Collier Cameron, A., Guenther, E., Smalley, B., McDonald, I., et al., 2010, *MNRAS*, 407, 507
- Crossfield, I. J. M., Ciardi, D. R., Petigura, E. A., Sinukoff, E., et al., 2016, *ApJS*, 226, 7
- Cumming, A., Butler, R. P., Marcy, G. W., Vogt, S. S., et al. 2008, *PASP*, 120, 531
- Currie, T., 2009, *ApJ*, 694, L171
- Eastman J., 2017, Astrophysics Source Code Library, ascl:1710.003
- Fisher, D. A., & Valenti, J., 2005, *ApJ*, 622, 1120
- Fuhrmann, K., Axer, M., & Gehren, T., 1993, *A&A*, 271, 451
- Gandolfi, D., Hébrard, G., Alonso, R., Deleuil, M., et al., 2010, *A&A*, 524, A55
- Gaudi, B. S., Stassun, K. G., Collins, K. A., Beatty, T. G., et al., 2017, *Nature*, 546, 514
- Hartman, J. D., Bakos, G. Á., Bhatti, W., Penev, K., et al., 2016, *AJ*, 152, 182
- Henden, A. A., Levine, S., Terrell, D., & Welch, D. L., 2015, *AAS*, 22533616H
- Ida, S., & Lin, D. N. C., 2004, *ApJ*, 616, 567
- Ida, S., & Lin, D. N. C., 2005, *ApJ*, 626, 1045
- Jackson, B., Greenberg R., & Barnes, R., 2008, *ApJ*, 678, 1396
- Johnson, J. A., Fischer, D. A., Marcy, G. W., Wright, J. T., et al. 2007, *ApJ*, 665, 785
- Johnson, J. A., Marcy, G. W., Fischer, D. A., Wright, J. T., et al. 2008, *ApJ*, 675, 784
- Johnson, J. A., Howard, A. W., Bowler, B. P., Henry, G. W., et al. 2010a, *PASP*, 122, 701J
- Johnson, J. A., Bowler, B. P., Howard, A. W., Henry, G. W., et al. 2010b, *ApJ*, 721L, 153J
- Johnson, J. A., Morton, T. D., & Wright, J. T., 2013, *ApJ*, 763, 53

- Kennedy, G. M., & Kenyon, S. J., 2008, *ApJ*, 673, 502
- Kipping, D. M., 2010, *MNRAS*, 407, 301
- Kovács, G., Bakos, G. & Noyes, R., 2005, *MNRAS*, 356, 557
- Kovács, G., Zucker, S. & Mazeh, T., 2002, *A&A*, 391, 369
- Leconte, J., Chabrier, G., Baraffe, I., & Levrard, B., 2010, *A&A*, 516, 64
- Lloyd, J. P., 2011, *ApJ*, 739, L49
- Lloyd, J. P., 2013, *ApJ*, 774L, 2L
- Lund, M. B., Rodriguez, J. E., Zhou, G., Gaudi, S., et al., 2017, *AJ*, 154, 194
- Maldonado, J., Villaver, E., & Eiroa, C., 2013, *A&A*, 554, 84
- Mandel, K., & Agol, E., 2002, *ApJ*, 580, L171
- Mayo, A. W., Vanderburg, A., Latham, D. W., Bieryla, A., et al., 2018, *AJ*, 554, 84
- McLaughlin, D. B., 1924, *ApJ*, 60, 22
- Meléndez, J., Bergemann, M., Cohen, J. G., Endl, M., et al., 2012, *A&A*, 543, A29
- Meléndez, J., Schirbel, L., Monroe, T. R., Yong, D., et al., 2014, *A&A*, 567, L3
- Mislis, D., & Hodgkin, S., 2012, *MNRAS*, 422, 1512M
- Mislis, D., Pyrzas, S., Alsubai, K. A., Tsvetanov, Z. I., & Vilchez, N. P. E. 2017, *MNRAS*, 465, 3759M
- Mordasini, C., Alibert, Y., Benz, W., Klahr, H., & Henning, T., 2012, *A&A*, 541, A97
- Morton, T. D., 2012, *ApJ*, 761, 6
- Morton, T. D., 2015, *VESPA*, False positive probability calculator, Astrophysics Source Code Library, ascl:1505.011
- Morton, T. D., Bryson, S. T., Coughlin, J. L., Rowe, J. F., et al., 2016, *ApJ*, 822, 86
- Murgas, F., Pallé, E., Parviainen, H., Chen, G., et al., 2017, *A&A*, 605, 114
- Narita, N., Fukui, A., Kusakabe, N., Watanabe, N., et al., 2018, *arXiv:1807.01908*
- Papaloizou, J. C. B., Nelson, R. P., Kley, W., Masset, F. S., & Artymowicz, P., 2007, *Protostars and Planets V*, eds. Reipurth, B., Jewitt, D. and Keil, K. (Tucson: University of Arizona Press), 655
- Pickles, A., & Depagne E., 2010, *PASP*, 122, 1437
- Pont, F., Moutou, C., Gillon, M., Udalski, A., et al., 2007, *A&A*, 465, 1069
- Queloz, D., Henry, G. W., Sivan, J. P., Baliunas, S. L., et al., 2001, *A&A*, 379, 279
- Reffert, S., Bergmann, C., Quirrenbach, A., Trifonov, T., & Künstler, A., 2015, *A&A*, 574, A116
- Ribas, Á., Bouy, H., & Merín, B., 2015, *A&A*, 576, A52
- Rodriguez, J. E., Zhou, G., Vanderburg, A., Eastman, J. D., et al., 2017, *AJ*, 153, 256
- Rossiter, R. A., 1924, *ApJ*, 60, 15
- Rowe, J., Borucki, W. J., Howell, S. B., Gilliland, R. L., et al., 2011, *AAS*, 21710304R
- Santos, N. C., Adibekyan, V., Figueira, P., Andreasen, D. T., et al., 2017, *A&A*, 603, 30S
- Schlafly E. F., & Finkbeiner D. P., 2011, *ApJ*, 737, 103
- Schlaufman, K. C., & Winn, J. N., 2013, *ApJ*, 772, 413
- Seager, S., & Mallén-Ornelas, G., 2003, *ApJ*, 585, 1038
- Sestito, P., & Randlich, S., 2005, *A&A*, 442, 615
- Snellen, I. A. G., Koppenhoefer, J., van der Burg, R. F. J., Dreizler, S., et al., 2009, *A&A*, 497, 545
- Talens G. J. J., Justesen, A. B., Albrecht, S., McCormac, J., et al., 2018, *A&A*, 612, 57
- Torres G., Konacki, M., Sasselov, D., & Jha S., 2005, *ApJ*, 619, 558
- Torres G., Andersen, J., & Giménez A., 2010, *A&ARv*, 18, 67
- Tucci Maia, M., Meléndez, J., Castro, M., Asplund, M., et al., 2015, *A&A*, 576, L10
- Villaver, E., Livio, M., Mustill, A. J., & Siess, L., 2014, *ApJ*, 794, 3
- Valenti, J. A., & Piskunov, N., 1996, *A&AS*, 118, 595
- Yi, S., Demarque, P., Kim Y.-C., Lee, Y.-W., et al., 2001, *ApJS*, 136, 417
- Zhou, G., Latham, D. W., Bieryla, A., et al., 2016, *MNRAS*, 460, 3376
- Zhou, G., Rodriguez, J. D., Collins, K. A., Beatty, T., et al., 2016, *AJ*, 152, 136
- Zhou, G., Bakos, G. A., Hartman, J. D., Latham, D. W., et al., 2017, *AJ*, 153, 211